Detailed numerical simulations of flow mechanics and membrane performance in spacer-filled channels, flat and curved

S. Wardeh[a], H.P. Morvan[b*]

[a]*Department of Civil Engineering,* [b]*Department of Mechanical, Manufacturing and Materials Engineering,*
Thermofluids Group, the University of Nottingham, UK
Tel. +44 (115) 951 3728; Fax +44 (115) 951 3800; email: herve.morvan@nottingham.ac.uk

ABSTRACT

Desalination by reverse osmosis is receiving increasing attention due to recent improvements in membrane technology in particular. This technique is now used for small to very large scale applications and has been identified as a key contributor to the Syrian water commission plans for example; there have also been comments in the British press about possible applications to the UK. Computational Fluid Dynamics (CFD) is increasingly used for complex modelling applications in the chemical process and water industries. In the present paper CFD is used to model desalination modules (channels and membranes) in which spacers are used to enhance mixing and maintain performance. In this work the fluid dynamics and the membrane physics are fully coupled. CFD offers bulk quantities, e.g. pressure, wall shear and mean salt accumulation on the membrane as already reported in part in [1], on the merits of various spacer setups but it also allows the computation of detailed maps for these values in the channel, along and across the membrane, which are the object of the paper. These maps permit the analysis of what is happening at the membrane level in great detail and could be used to further refine the channel and spacer setups. Whilst most of the experimental and CFD work done on these issues appears to have been done for flat channels, including in the present work, preliminary results are also included to report on the effects of curvature on the membrane performance.

Keywords: Desalination; Pressure-driven membrane; Concentration polarization; Spacers; Computational fluid dynamics (CFD)

1. Introduction

The modelling of flow or concentration polarisation on membrane surfaces is not new. Several simplified models have appeared in the literature over the past 40 years. Some of them demonstrated the importance of feed-side boundary layer resistance on the selectivity and capacity of the separation process [2,3]. Others investigated the concentration polarization phenomena for membrane systems [4,5] or looked at the effect of vari-

able permeation [6–10], changes in salt rejection [6,10], the effect of wall slip [11,12] and gravitational effects [13].

Since the late 1990s, computational fluid dynamics (CFD) has been more widely used in the chemical process industry and in related fields. Concentration polarization effects have thus been studied. Hansen et al. [14] investigated the velocity field for a channel with a permeate flow through a wall based on a concentration-dependent viscosity and on static and osmotic pressure differences. Geraldes et al. [15] also predicted water fluxes through a membrane in a simple channel. They considered that the variation of the solutions' properties, such

* Corresponding author.

as density, viscosity and diffusivity, is changed with the solutes concentrations. But, gravity effects were not considered [16]. Huang and Morrissey [17] simulated the development of concentration polarization in the membrane flow channel during an ultra-filtration process. This work was limited as the velocity field was assumed to have constant properties.

Wiley and Fletcher [18] modelled the concentration polarisation and fluid flow in pressure-driven membrane separation processes. The transport properties were considered to be a function of the concentration. They also investigated spacers using a crude rectangular geometry for the spacers. Further work was done to explore the effect of buoyancy in salt–water systems under reverse osmosis (RO) conditions [19]. Insights into the effect of spacer filaments on flow patterns in narrow channels of spiral-wound membrane modules were later obtained using the same approach [20].

Shock and Miquel [21] worked on various commercial spacers experimentally. They also used a computational approach to calculate the performance of different possible designs and highlighted the effect of permeate flow channel length and reported that there is an optimal number of membrane leaves to achieve reduction in pressure losses in the permeate channel.

Along similar lines, but numerically, Schwinge et al. [22,23] examined the effects of the Reynolds number, mesh length, and filament diameter on the mass transfer enhancement for several spacer configurations. Their simulation results revealed that, in general, spacer performance increases with the increase in the ratio of mass-transfer enhancement to pressure loss. Overall, they concluded that the zigzag spacer is the most efficient spacer type for a spiral-wound membrane module, something the authors also found [1]. They later looked at the effects of the spacers on the unsteady flow behaviour in narrow spacer filled channel [24]. The flow was simulated for several filament configurations and for different Reynolds numbers up to 2,000. Those simulations revealed that the transition to turbulent flow happened for Reynolds numbers between 200 and 800 depending on the filament configuration; this was also later confirmed in [1].

Results obtained by Li et al. [25] showed that mass transfer between neighbouring filaments is affected by the transient shedding of vortices, increasing mass transfer. They concluded that mass transfer optima as a function at certain values of l/h, where l is the filament spacing and h is the channel height. A ratio of 1/4 was found to be optimal. This is why the present contribution focuses on such an arrangement.

However, the above papers [21–23,25–29], and many others, discussed the flow patterns for a single fluid in a spacers filled channel with double sided walls (no membrane). Therefore, a lot of the available knowledge focuses on the fluid dynamics of spacer-filled channels,

with no attempt at modelling salt transport, deposition or permeation into the freshwater channels. This gap was bridged by the present authors in their recent paper on the effects of spacers on the fluid mechanics in flat channels, with double sided membranes [1]. They were able to provide clear figures on pressure loss, overall shear forces and salt accretion, as well as production efficiency for different spacer setups and for a range of Reynolds numbers.

The present contribution is an extension of the previous work. It has two aims: The first is (1) to provide more insight into the membrane performance itself, via detailed maps for the shear stress along the membrane and associated analysis of the permeate flow; and the second is (2) to take advantage of this to then examine the effects of channel curvature, as industrially reverse osmosis desalination devices are typically implemented in spiral-wound modules.

The lead author's interest in this research was prompted by the recent decision of the Syrian water commission to use desalination by reverse osmosis, which justified the development of knowledge in this area in order to implement suitable and sustainable solutions.

2. Case description, modelling assumptions and numerical methods

CFD simulations have been carried out for fluid flow through rectangular channels filled with several different spacer structures, Wardeh and Morvan [1]. It presented and validated a mathematical model of a membrane which was used to model desalination channels with and without spacers. This first paper focussed on the bulk performance found in such channels, viz. pressure loss, mean overall wall shear and salt mass fraction. The outcome of this research work is further detailed here where we report on the detailed effects of spacer filaments configurations on reducing salt accumulation along the membrane surface and enhancing water permeation by presenting maps of these values along the membrane in conjunction with an analysis of the flow dynamics in the channel. The current paper also aims to consider the potential effects of the channel curvature on the membrane performance.

The following filament configurations were used d/h = 0.5, l/h = 4, Fig. 2 , with Reynolds numbers up to 800. The feed channel was given sufficiently long entrance and exit lengths in order to allow for a fully-developed flow to form before entering the channel and to avoid interference between the recirculation region behind the last spacer and the channel exit. The geometry used is the same as in Wardeh and Morvan [1] and is shown in Fig. 1. In the simulations, L was set to 49.5 mm. The inlet and exit are located at Lin = –12 mm and Lout = 74.5 mm.

Various spacer arrangements exist and have received attention in the literature; among the most successful are
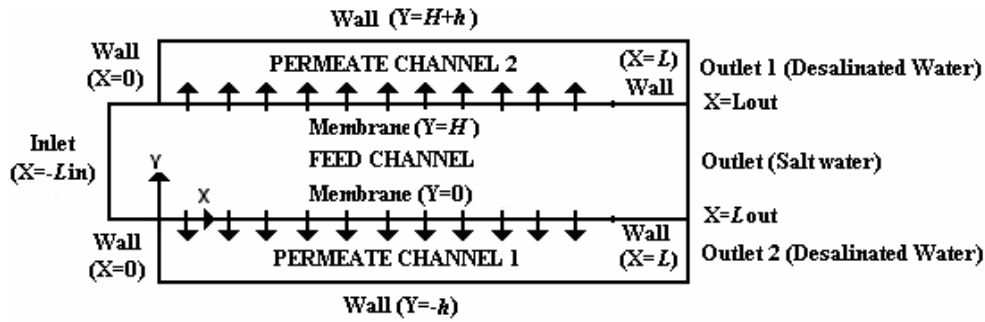
Fig. 1. A schematic of the two sided membrane geometry considered in the simulations.
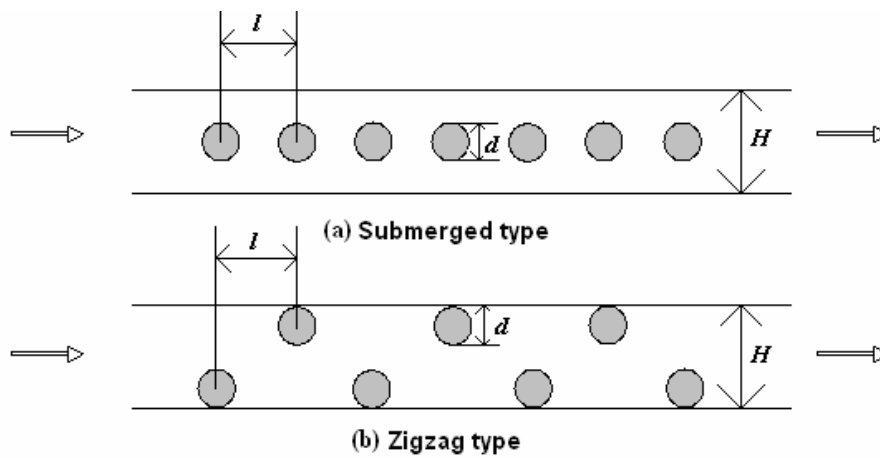
Fig. 2. Transverse spacer filaments configurations used in the feed channel.

the submerged and the zigzag types, Fig. 2a and Fig. 2b, respectively. Their success is due to their ability to produce the most homogenous performance in terms of wall shear on both sides of the channel and justifies their selection in our study. The total number of spacers in each case has been taken as seven as it was demonstrated in [29] that a minimum of six spacers in the channel is sufficient to develop the unsteady flow patterns in the configurations of interest here.

The definition for the channel Reynolds number had to be slightly modified to consider the changes in the hydraulic diameter d_h and voidage, ε, due to the existence of spacer filaments [23].

$$\text{Re}_{ch} = \frac{d_h \cdot U_{av}}{\nu} \tag{1}$$

where U_{av} is the average velocity in the channel.

The hydraulic diameter d_h is defined as

$$d_h = \frac{4\varepsilon}{\dfrac{2}{h_{ch}} + (1-\varepsilon)S_{vsp}} \tag{2}$$

h_{ch} is the channel height and S_{vsp} is calculated as

$$S_{vsp} = \frac{S_{sp}}{V_{sp}} = \frac{4}{d} \tag{3}$$

where d is the spacer diameter in m.

The voidage ε is

$$\varepsilon = \frac{V_{tot} - V_{sp}}{V_{tot}} \tag{4}$$

where V_{sp} is volume of a channel containing spacers and V_{tot} is volume of the spacers present in the channel.

The flow solution relies on the Navier–Stokes equations for a multi-component-flow (salt and water); these are solved for the setup described above using the CFX-ANSYS multigrid solver following a finite volume formulation. Significant user-FORTRAN was implemented to account for the membrane physics, which was fully validated in the authors previous paper [1]. The same numerical method as described in Wardeh and Morvan [1] was implemented here to compute both the flow through the channel, over and through the membrane. A second-order backward Euler method is used for the transient scheme and all the simulations are carried out using double precision arithmetic in order to avoid prob-

lems with round off errors. A time step dependence study was undertaken to determine the effect of the time step size on the accuracy of the results. This was done by choosing a time step size of the order of the timescales of interest, and then running a fixed but small period of the simulation in physical time. Then the run is repeated for the same period using double and half this time step size, and the results compared. The chosen time step for each run was small enough to resolve the unsteady flow and it was established that it needed to be smaller than 0.1 ms in order to achieve convergence at each time step at $Re_{ech} = 800$ for example. This leads to computational times of several weeks for each transient simulation on a single CPU. At each time step, convergence was achieved in less than 20 iterations with a residual target of 10^{-5} ensuring a high degree of convergence.

3. Results and discussion

3.1. Previous work and overview of results

It was previously established that the use of spacer filaments in such a narrow flow channel increases the pressure loss because of the additional drag force caused by each spacer filament. These losses were quantified in [1] for the two optimized setups presented here. Further validation results on the flow dynamics are shown in Fig. 3, together with a more complete and previously unpublished table of the overall channel performance, Table 1, for different spacer setups and at various Re values.

Regarding the flow dynamics, the transient nature of the flow beyond Re = 200, noted by Schwinge and his team is seen to have been accurately replicated, Fig. 4. This is important as some recent studies were still conducted using steady state simulations, including at Re

values larger than those presented here for similar channels; see [30] for example.

Table 1 summarises the authors' findings. It shows that the gain in permeate flow rate per unit area is typically about 30% compared to an empty channel for the cases reported here and that, in general, the cross flow gets proportionally higher with spacers (up to 40% gain) compared to the empty channel configuration. It is clear that spacers have an important effect on the flow in the feed channel and across the membrane, with the zigzagging spacer filaments type giving, overall, the lowest salt concentrations at the membrane surface and the highest permeate flow for most of Reynolds numbers for example.

It should be noted that the submerged spacer type performs better than the zigzagging type at the highest Reynolds number though, but that this performance comes at a cost because the gauge pressure required to achieve this is up by 70% [1]. In other words, for the same value of pressure drop, the submerged-type spacers create a higher shear stress on the membrane wall compared with that created by the zigzagging type spacers. However, the overall shear stress produced by the submerged type spacers appears to be less efficient in preventing the accumulation of salt accumulated on the membrane surface and therefore this alone does not constitute a good criterion to select a channel and spacer configurations. Since it is vital to achieve a high mass transfer rate at the lowest possible pressure loss in order to optimise the reverse osmosis process and to reduce operational costs, the so-called zigzagging type appears to be the desirable option even at the higher Reynolds numbers.

The work presented next aims to investigate these points in more depth, in particular by analysing the link between the flow dynamics in the channel, resulting shear stress values, salt concentrations and permeation velocities at and along the membrane.

Current simulations   Schwinge et al, 2003
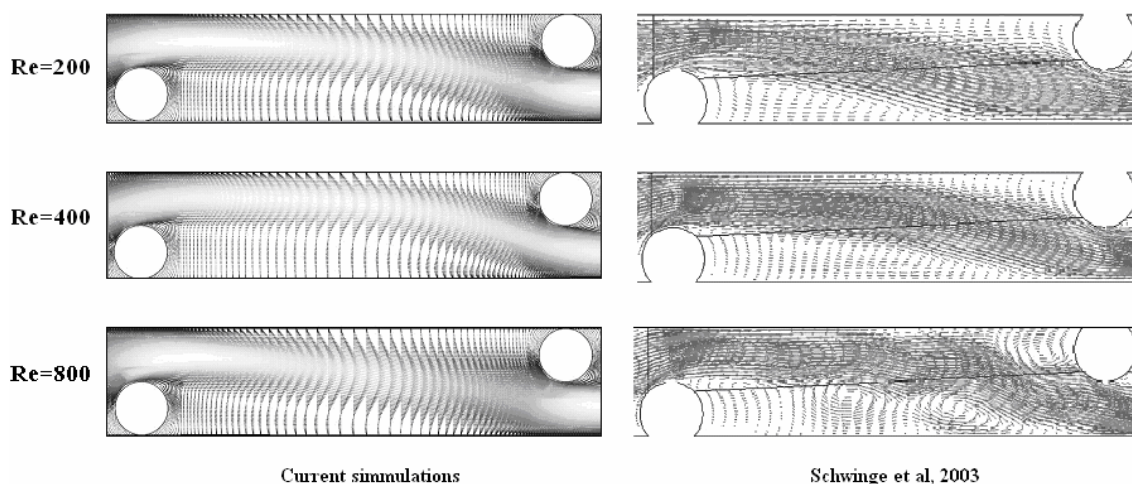
Fig. 3. Unsteady flow for Re_{ch} ranging from 100 to 800 for multiple filaments located alternately adjacent to the top and bottom walls.
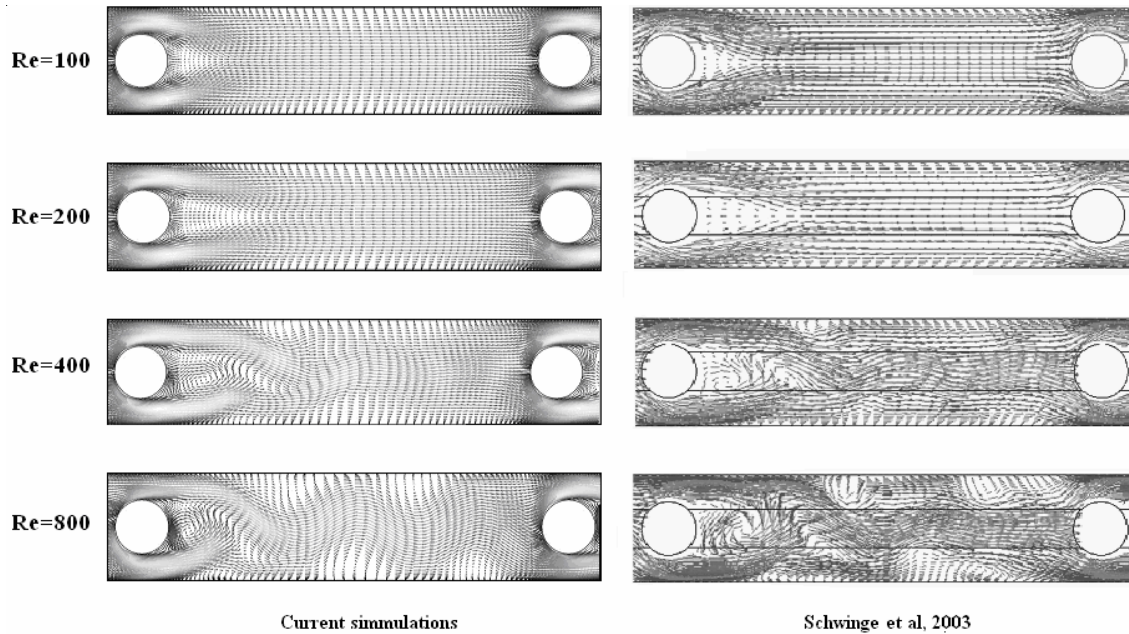
Fig. 4. Unsteady flow for Re$_{ch}$ ranging from 100 to 800 for multiple filaments located in the centre of the channel.

Table 1
Average values of gauge pressure, wall shear, salt mass fraction and permeation velocity on the feed side membrane at (Y = 0) for double sided membrane channel

Statistical characteristics		Empty channel	Zigzagging type spacers	Submerged type spacers
Re = 100	Gauge pressure, Pa	5.36E + 00	1.41E + 01	2.37E + 01
	Wall shear, Pa	5.88E − 02	7.49E − 02	1.53E − 01
	Wall shear X, Pa	−5.88E − 02	−6.48E − 02	−1.53E − 01
	Wall shear Y, Pa	1.25E − 19	−1.87E − 09	9.93E − 20
	Salt mass fraction	5.60E − 03	5.37E − 03	5.39E − 03
	Permeation velocity, m s^{-1}	1.44E − 05	1.78E − 05	1.76E − 05
Re = 200	Gauge pressure, Pa	1.13E + 01	3.53E + 01	5.94E + 01
	Wall shear, Pa	1.18E − 01	1.64E − 01	3.48E − 01
	Wall shear X, Pa	−1.18E − 01	−1.19E − 01	−3.48E − 01
	Wall shear Y, Pa	1.53E − 19	−6.09E − 09	1.39E − 19
	Salt mass fraction	5.39E − 03	5.04E − 03	5.12E − 03
	Permeation velocity, m s^{-1}	1.75E − 05	2.27E − 05	2.17E − 05
Re = 400	Gauge pressure, Pa	2.52E + 01	9.23E + 01	1.62E + 02
	Wall shear, Pa	2.38E − 01	4.05E − 01	7.44E − 01
	Wall shear X, Pa	−2.38E − 01	−2.38E − 01	−7.22E − 01
	Wall shear Y, Pa	1.86E − 19	−1.89E − 08	2.36E − 19
	Salt mass fraction	5.16E − 03	4.60E − 03	4.65E − 03
	Permeation velocity, m s^{-1}	2.10E − 05	2.94E − 05	2.77E − 05
Re = 800	Gauge pressure, Pa	6.00E + 01	2.85E + 02	4.89E + 02
	Wall shear, Pa	4.77E − 01	1.03E + 00	1.98E + 00
	Wall shear X, Pa	−4.77E − 01	−5.54E − 01	−1.54E + 00
	Wall shear Y, Pa	2.23E − 19	−5.09E − 08	3.01E − 19
	Salt mass fraction	4.90E − 03	4.26E − 03	4.16E − 03
	Permeation velocity, m s^{-1}	2.50E − 05	3.47E − 05	3.53E − 05

Fig. 5. Wall shear stress on the feed side of the membrane for Re = 100.
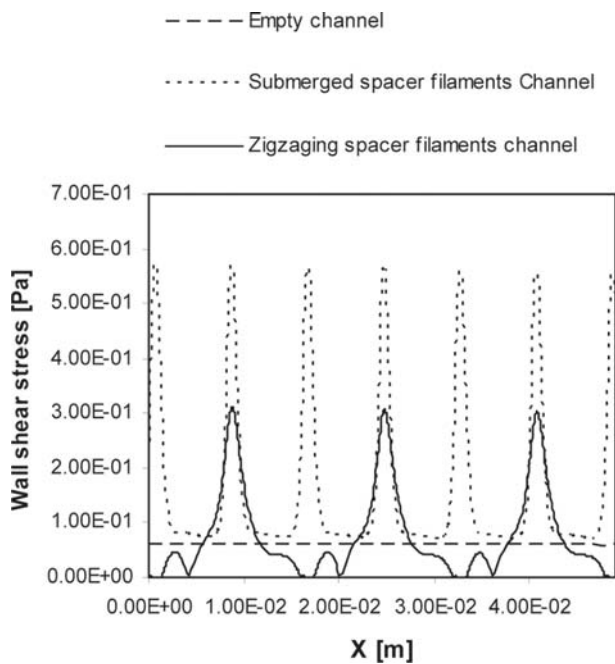
Fig. 6. Salt mass fraction on the feed side of the membrane for Re = 100.

Fig. 7. Permeation velocity across the feed side of the membrane for Re = 100.
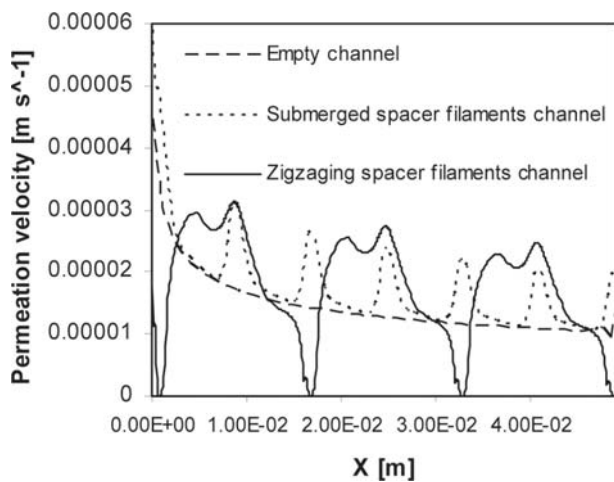
Fig. 8. Wall shear stress on the feed side of the membrane for Re = 200.

3.2. Detailed shear stress, mass fraction and permeation velocity maps

Maps of shear stress, salt concentration and permeation velocities are presented here. The plots are taken along the bottom membrane in Fig. 2 and presented in a group of three for each Re value.

In the case of zigzagging-type spacers, high shear stress levels occur in areas close to the spacers, longitudinally, but on the opposite side of the membrane with respect to the spacer position; the shear stress is actually low in the immediate vicinity of the spacers, Figs. 5, 8, 11 and 14, resulting in important localised salt deposition on the membrane, in what is effectively a dead zone, and corresponding low permeation velocities across the membrane, Figs. 7, 10, 13 and 17. It should also be noted that the recirculation seen in the wake of the spacer, Fig. 3, results, for this configuration, in secondary shear stress peaks seen "upstream" of the large peaks, in Fig. 5 for example. As the Re increases these secondary peaks in-
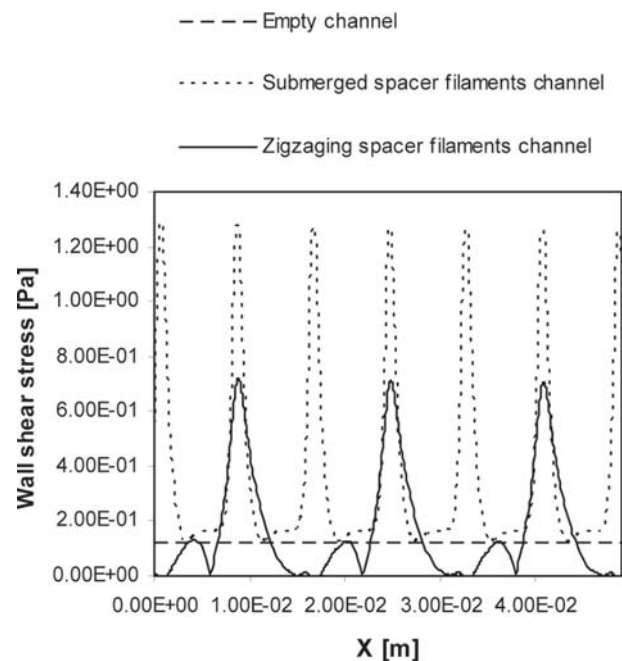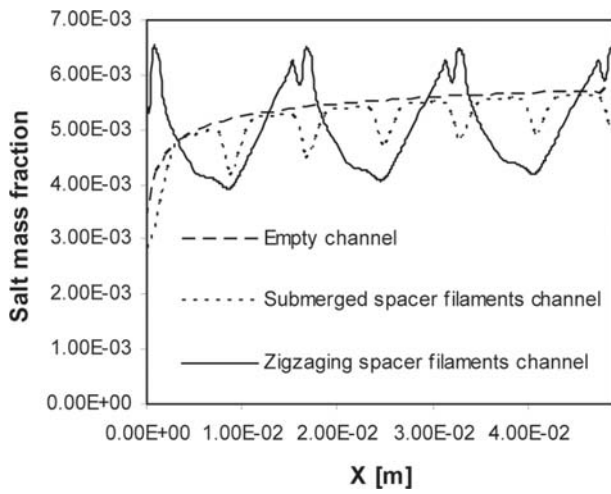
Fig. 9. Salt mass fraction on the feed side of the membrane for Re = 200.
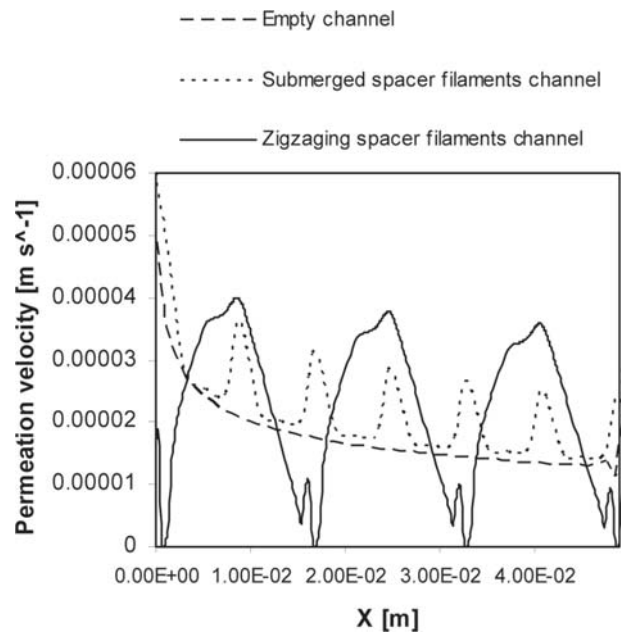
Fig. 10. Permeation velocity across the feed side of the membrane for Re = 200.
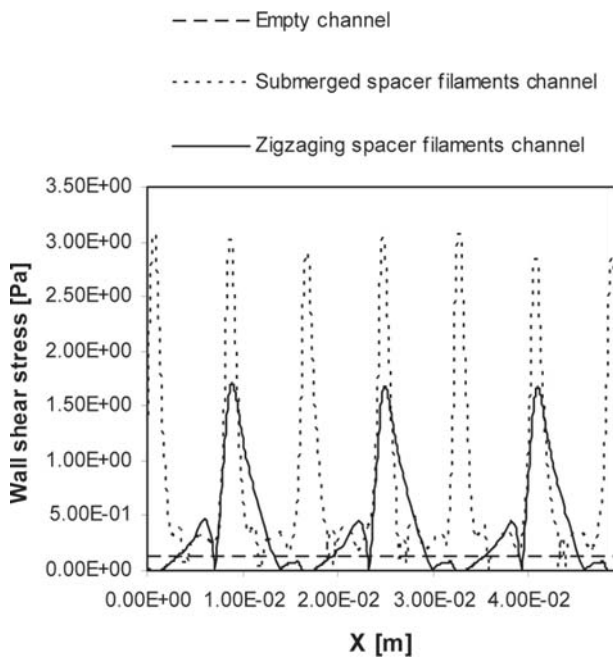
Fig. 11. Wall shear stress on the feed side of the membrane for Re = 400.
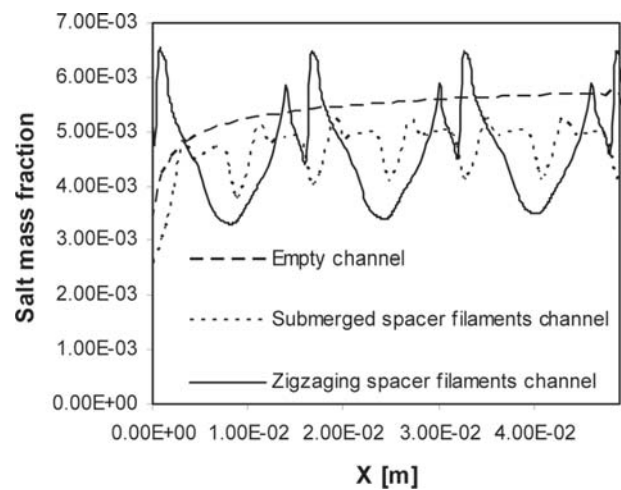
Fig. 12. Salt mass fraction on the feed side of the membrane for Re = 400.

crease, Fig. 8, Fig. 11 and Fig. 14 for example. This highlights the sweeping effect that takes place in the channel and which results in regions of low salt concentration behind the spacers (about half a diameter away, Fig. 15): up to and including the case Re = 200 two corresponding troughs are visible in Fig. 6 and Fig. 9 for the salt concentration; at higher Re values this effect stretches to the whole wake region, up to the following spacer, for the configuration adopted here. Following the same trends, the permeation velocity reflects perfectly the state of the

membrane surface, and two peaks are visible up to Re = 200 for example in Fig. 7 and Fig. 10.

In the case of submerged spacers, the areas of high shear stress on the membrane surface are found close to the spacers, on both sides of the channel, in the form of much localised, sharp peaks. Corresponding to these sharp peaks are equally localised reductions in salt concentration, which, at low Re numbers in particular, are unspectacular and lead to low improvements in permeation velocities over the empty channel configuration,
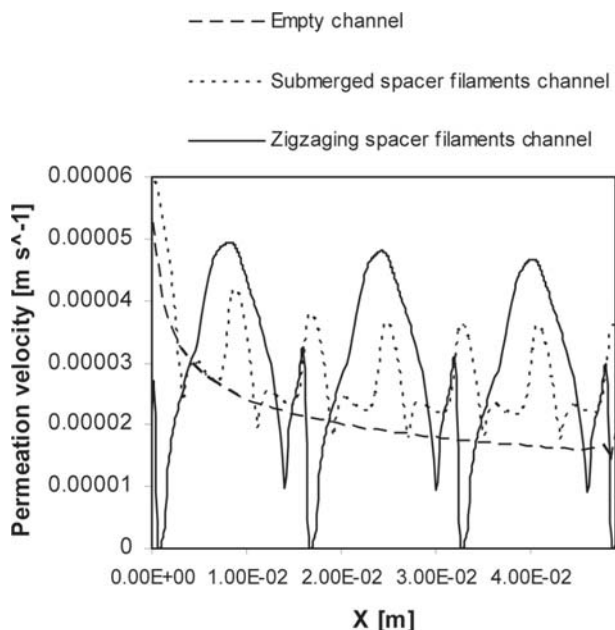
Fig. 13. Permeation velocity across the feed side of the membrane for Re = 400.
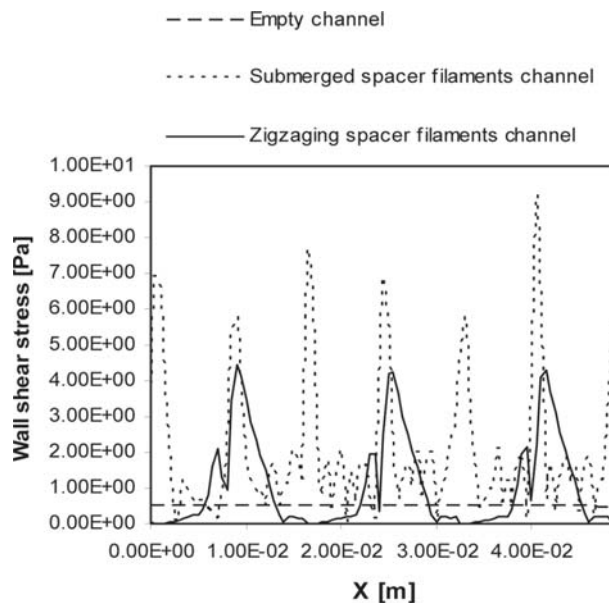
Fig. 14. Wall shear stress on the feed side of the membrane for Re = 800.
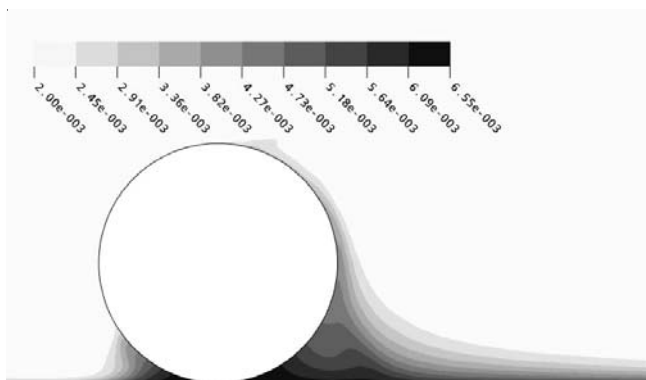
Fig. 15. Salt accumulation around a spacer located on the membrane surface for Re = 800. Scale in volume fraction [%].
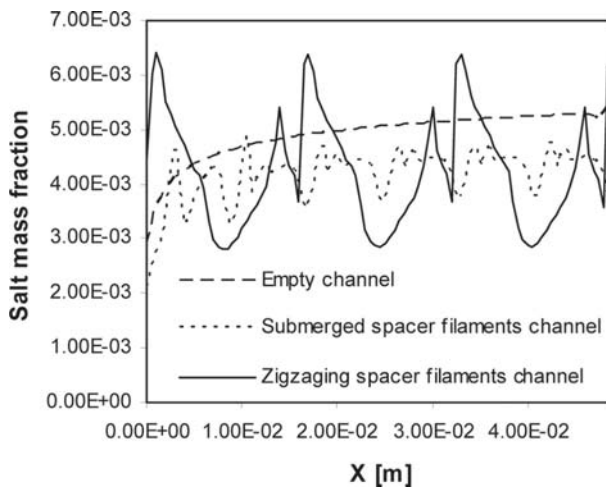
Fig. 16. Salt mass fraction on the feed side of the membrane for Re = 800.

Figs. 7, 10 and 13. Submerged type spacers do produce a more uniform pattern (something desirable in principle) of premeate flow but do not perform as well overall, as visible in Table 1. They do not perform well because the shear peak is too localised and that great regions of the membrane do not benefit from substantial surface sweeping. The zigzagging-type setup clearly has a marked advantage because it results in a broader region of shear and much improved permeation velocities; this advantage becomes particularly noticeable when energy considerations (pressures) are also taken into account, Table 1.

4. Curvature effects

Most of the numerical studies available in the literature (if not all of them) have investigated the flow in rectangular flat channels. However, in industrial spiral-wound modules, membrane-envelopes are wrapped around a central tube. This implies that the membranes are curved, and the curvature for each membrane layer increases with the distance from the centre. It is not yet possible to model these modules in 3D [1] but it would be possible to evaluate the performance of these modules numerically by running simulations for channels
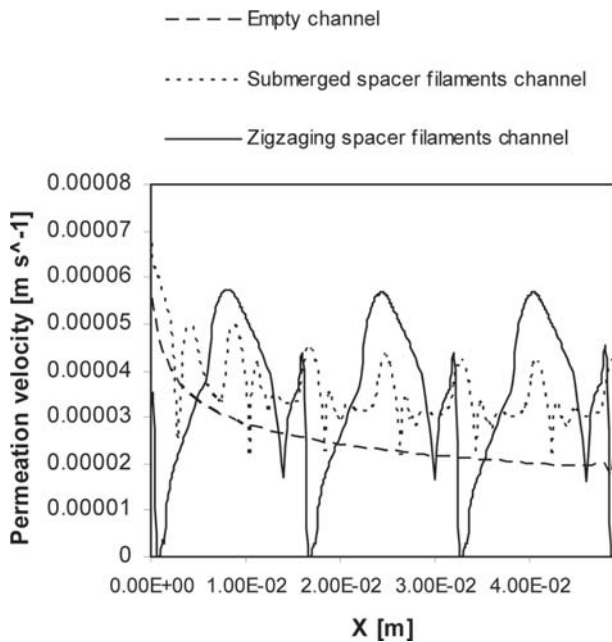
Fig. 17. Permeation velocity across the feed side of the membrane for Re = 800.

Fig. 18. Geometry with curvature.

with different values of curvature. Each curvature value would represent the curvature for a membrane layer for example.

What is proposed here is not to run and report on a large number of cases but to assess the potential impact of curvature on the setup investigated by the authors, in particular the rather successful zigzagging one, and to do so in light of the analysis provided in section 3. The flow around zigzagging filaments, in single and double sided membrane channels, was therefore computed. The diameter of curvature is taken as 10 cm, Fig. 18, and a modest Reynolds number of 100 is investigated first. The idea is that, should significant changes be noted at this low Re value, the impact at operating levels of several hundreds is likely to be significant as transient flow structures develop to combine with centrifugal effects. The boundary and the initial conditions employed for this simulation are similar to those used in modelling the flat channel cases reported in [1] and here above.

Table 2 shows that in the case of a channel with curvature, the average value of the mean wall shear stress on the membrane wall increases by about 34%, compared with that for a flat channel. The reduction of the salt mass fraction is only about 2% though, and the permeate flow rate per unit area is typically of about 10%. This increase in the mean shear stress does not seem to have a large influence on the salt concentration, yet is slightly more noticeable on the permeation velocity on the membrane wall and is likely to increase at higher Reynolds values.

Figs. 19–21 examine in greater detail the effects of curvature on the wall shear stress, on the inner membrane side, and the reduction in salt mass fraction along
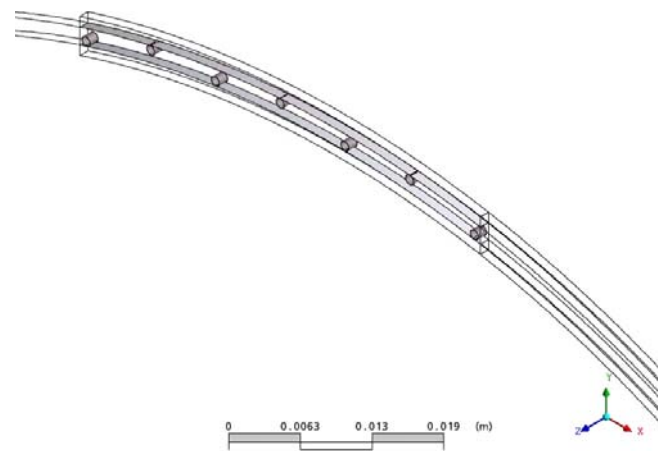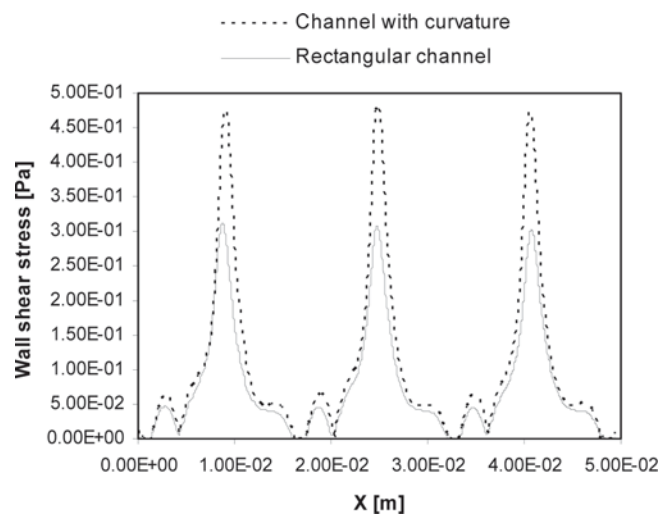
Fig. 19. Wall shear stress on the feed side of the membrane at (Y = 0).

the membrane and permeation velocity, on the feed side, compared with a flat channel for a Reynolds number of 100. It can be seen in Fig. 19 that the wall shear stress increases mainly in areas close to the spacers, but on the opposite side membrane. In the flat channel case, the high shear stress occurs in the same areas, at similar Re numbers. Little difference is noticeable on the outer side, Figs. 22–24, at this Re value however, the ratio between channel height and curvature being rather small. Where this ratio is increased and for higher Re, this may change, but this is likely to be limited to specific areas which may not be representative of a significant percentage of the membrane surface.

Table 2
Average values of gauge pressure, wall shear, salt mass fraction and permeation velocity on the feed side membrane at ($Y = 0$) for double sided membrane channel

Statistical characteristics	Flat channel	Channel with curvature	Percentage of difference (%)
Gauge pressure, Pa	14.54E + 00	22.30 E + 00	53.39
Wall shear stress, Pa	7.49E − 02	1.00E − 01	34.20
Salt mass fraction at ($Y = 0$)	5.37E − 03	5.25E − 03	−2.20
Permeation velocity, m s^{-1}	1.78E − 05	1.96E − 05	10.13
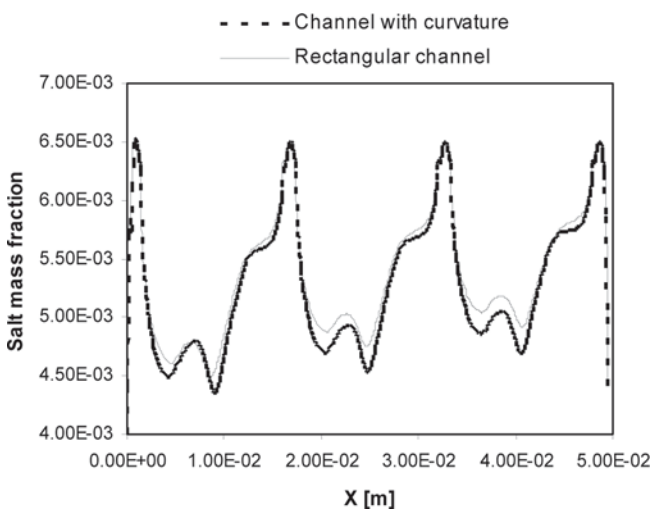
Fig. 20. Salt mass fraction on the feed side of the membrane at ($Y = 0$).
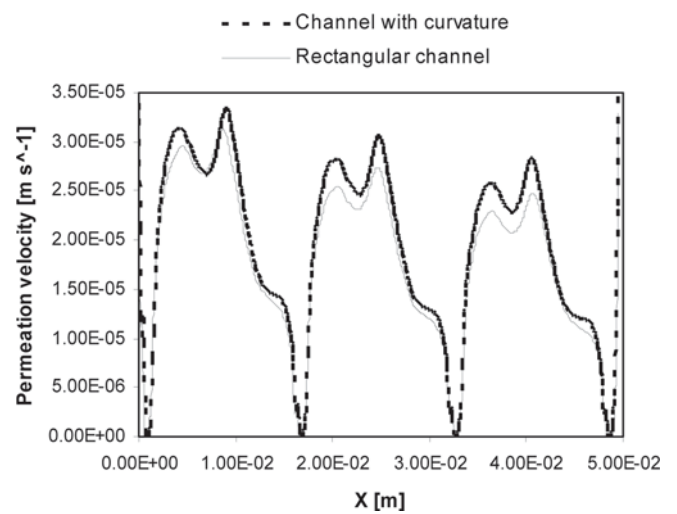
Fig. 21. Permeation velocity across the feed side of the membrane at ($Y = 0$).
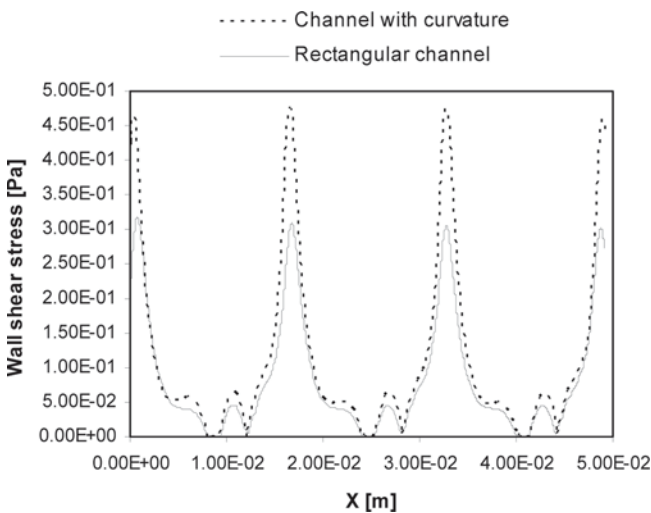
Fig. 22. Wall shear stress on the feed side of the membrane at ($Y = H$).
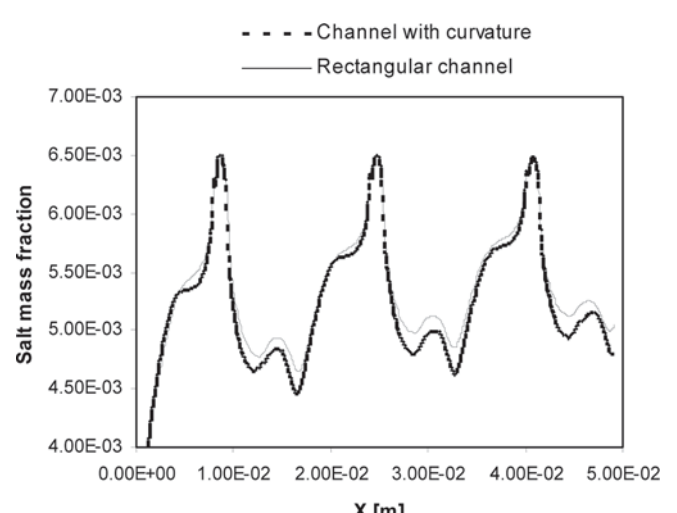
Fig. 23. Salt mass fraction on the feed side of the membrane at ($Y = H$).
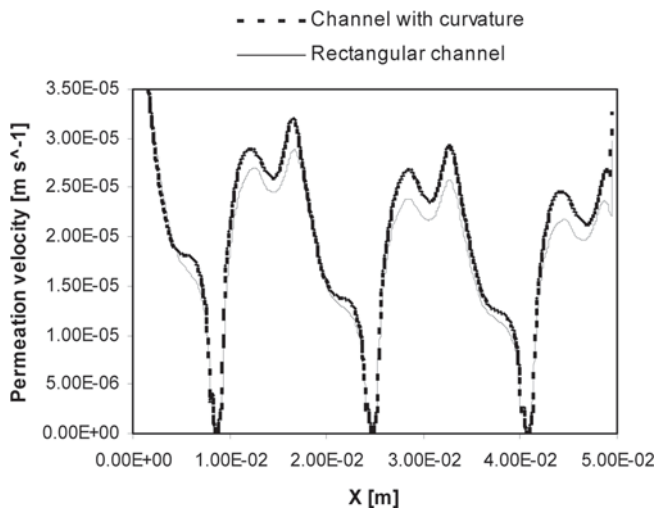
Fig. 24. Permeation velocity across the feed side of the membrane at ($Y = H$).

5. Conclusions

A computational model has been developed to investigate water flux and concentration polarization in membrane systems. The commercial code ANSYS-CFX was used with significant user FORTRAN to investigate membrane processes, such as shear stress, salt accumulation and permeation velocities following validation of the membrane model in [1]. The simulations reveal the detailed flow patterns, as well as bulk pressure losses and wall shear stresses, and looks at the effects of the spacer filaments in cleaning the precipitated salt accumulated on the membrane surface and on its performance. Results suggest that the zigzagging type is more economical and more efficient in removing accumulated salt from the membrane surface compared with the submerged one.

A thorough analysis of the detailed physics taking place at the membrane level has been carried out and reveals that the issue with the submerged arrangements in the configuration and at the Re values studied here is related to a high, yet very localised peak of shear stress which does not result in significant salt removal along the membrane. The advantage of the zigzagging configuration is that a broader shear stress zone is created, which results in lower salt concentrations on the membrane and higher permeation velocities, all of which is achieved at low cost (pressure).

Further work on the effect of curvature also indicates that although shear stress can be significantly increased by curvature, salt accumulation remains broadly unaffected at the Re number tested here and the permeation velocity only increases slightly. However it could be more significant at higher Re and in areas of tighter curvature, and further work is needed to ascertain this fully.

The main drawback of the present work is its computational cost. Work is therefore ongoing to approximate the spacers by a porous medium model to reduce the computational cost. Early results indicate that the statistical (bulk) characteristics obtained from the porous medium model are very close to those obtained form spacers filled geometry for all Reynolds numbers and will be examined against the results presented here once the work is complete. However this new model will only be good to evaluate mean properties and cannot replace the detailed work presented here as complex flow dynamics is removed from the solution in the absence of physical spacer in the solution.

References

[1]   S. Wardeh and H.P. Morvan, CFD simulations of flow and concentration polarization in spacer-filled channels for application to water desalination. IChemE J., 2008, in press.
[2]   A.S. Michaels, Effects of feed-side solute polarization on pervaporative stripping of volatile organic solutes from dilute aqueous solution: a generalized analytical treatment, J. Membr. Sci., 101 (1995) 117–126.
[3]   S. Bhattacharya and S.T. Hwang, Concentration polarization, separation factor, and Peclet number in membrane processes, J. Membr. Sci., 132 (1997) 73–90.
[4]   A.L. Zydney, Stagnant film model for concentration polarization in membrane systems, J. Membr. Sci., 130 (1997) 275–281.
[5]   S.P. Agashichev, Modelling concentration polarization phenomena for membrane channel with cylindrical geometry in an ultrafiltration process, Desalination, 119 (1998) 159–168.
[6]   T. Kotzev, Numerical study of the fluid dynamics and mass transfer of an ultrafiltration performance in a tube membrane module, Intern. J. Eng. Sci., 32 (1994) 359–368.
[7]   W.N. Gill, C. Tien and D.W. Zeh, Analysis of continuous reverse osmosis systems for desalination, Intern. J. Heat Mass Transfer, 9(9) (1966) 907–923.
[8]   A.A. Kozinski, F.P. Schmidt and E.N. Lightfoot, Velocity profiles in porous-walled ducts, Ind. Eng. Chem. Fundam., 9(3) (1970) 502–505.
[9]   W.N. Gill, C. Tien and D.W. Zeh, Concentration polarization effects in a reverse osmosis system, Ind. Eng. Chem. Fundam., 4(4) (1965) 433–439.
[10] P.L.T. Brian, Concentration polarization in reverse osmosis desalination with variable flux and incomplete salt rejection, Ind. Eng. Chem. Fundam., 4(4) (1965) 439–445.
[11] R. Singh and R.L. Laurence, Influence of slip velocity at a membrane surface on ultrafiltration performance — I. Channel flow system, Intern. J. Heat Mass Transfer, 22(5) (1979) 721–729.
[12] H.M. Yeh and T.W. Cheng, Analysis of the slip effect on the permeate flux in membrane ultrafiltration, J. Membr. Sci., 154 (1999) 41–51.
[13] K.H. Youm, A.G. Fane and D.E. Wiley, Effects of natural convection instability on membrane performance in dead-end and cross-flow ultrafiltration, J. Membr. Sci., 116 (1996) 229–241.
[14] M. Hansen, V.A. Barker and O. Hassager, Spectral element simulation of ultrafiltration, Chem. Eng. Sci., 53(17) (1998) 3099–3115.
[15] V.M. Geraldes, V.A. Semiao and M.N. de Pinho, Nanofiltration mass transfer at the entrance region of a slit laminar flow, Ind. Eng. Chem. Res., 37(12) (1998) 4792–4800.
[16] V.M. Geraldes, V.A. Semiao and M.N. de Pinho, Flow and mass transfer modelling of nanofiltration, J. Membr. Sci., 191 (2001) 109–128.
[17] L. Huang and M.T. Morrissey, Finite element analysis as a tool

for crossflow membrane filter simulation, J. Membr. Sci., 155 (1999) 19–30.

[18] D.E. Wiley and D.F. Fletcher, Techniques for computational fluid dynamics modelling of flow in membrane channels, J. Membr. Sci., 211 (2003) 127–137.

[19] D.F. Fletcher and D.E. Wiley, A computational fluids dynamics study of buoyancy effects in reverse osmosis, J. Membr. Sci., 245 (2004) 175–181.

[20] J. Schwinge, D.E. Wiley and D.F. Fletcher, A CFD study of unsteady flow in narrow spacer-filled channels for spiral-wound membrane modules, Desalination, 146 (2002) 195–201.

[21] G. Schock and A. Miquel, Mass transfer and pressure loss in spiral wound modules, Desalination, 64 (1987) 339–352.

[22] J. Schwinge, D.E. Wiley and D.F. Fletcher, Simulation of the flow around spacer filaments between channel walls. 2. Mass-transfer enhancement, Ind. Eng. Chem. Res., 41(19) (2002) 4879–4888.

[23] J. Schwinge, D.E. Wiley and D.F. Fletcher, Simulation of the flow around spacer filaments between narrow channel walls. 1. Hydrodynamics, Ind. Eng. Chem. Res., 41(12) (2002) 2977–3011.

[24] J. Schwinge, D.E. Wiley and D.F. Fletcher, Simulation of unsteady flow and vortex shedding for narrow spacer-filled chan-

nels, Ind. Eng. Chem. Res., 42 (2004) 4962–4977.

[25] F. Li, W. Meindersma, A.B. de Haan and T. Reith, Optimization of commercial net spacers in spiral wound membrane modules, J. Membr. Sci., 208 (2002) 289–302.

[26] Z. Cao, D.E. Wiley and A.G. Fane, CFD simulations of net-type turbulence promoters in a narrow channel, J. Membr. Sci., 185 (2001) 157–176.

[27] C.P. Koutsou, S.G.Yiantsios and A.J. Karabelas, Numerical simulation of the flow in a plane-channel containing a periodic array of cylindrical turbulence promoters, J. Membr. Sci., 231 (2004) 81–90.

[28] V.M. Geraldes, V.A. Semiao and M.N. de Pinho, The effect of the ladder-type spacers configuration in NF spiral-wound modules on the concentration boundary layers disruption, Desalination, 146 (2002) 187–194.

[29] J. Schwinge, D.E. Wiley and D.F. Fletcher, Simulation of unsteady flow and vortex shedding for narrow spacer-filled channels, Ind. Eng. Chem. Res., 42 (2003) 4962–4977.

[30] M. Gimmelshtein and R. Semiat, Investigation of flow next to membrane walls, J. Membr. Sci., 264 (2005) 137–150.